phys. stat. sol. (a) **205**, No. 4, 779–783 (2008) / **DOI** 10.1002/pssa.200777904

physica status solidi a
www.pss-a.com
applications and materials science

The optical Hall effect

T. Hofmann[*,1], **C. M. Herzinger**[2], **C. Krahmer**[3], **K. Streubel**[3], **and M. Schubert**[1]

[1] Department of Electrical Engineering and Nebraska Center for Materials and Nanoscience, University of Nebraska-Lincoln, USA
[2] J.A. Woollam Co., Inc., 645 M St. #102, Lincoln, NE 68508, USA
[3] Osram Opto Semiconductors, Wernerwerkstr. 2, 93049 Regensburg, Germany

Received 13 October 2007, revised 1 February 2008, accepted 6 February 2008
Published online 26 March 2008

PACS 71.18.+y, 78.20.Ls, 78.30.Fs

* Corresponding author: e-mail thofmann@engr.unl.edu

Classic electrical Hall effect measurements are standard for electrical characterization of free charge carriers in semiconductor layer structures. We demonstrate that magnetooptic generalized ellipsometry at long wavelengths when applied to conducting or semiconducting multilayer or nanoscopically in-homogeneous structures can yield equivalent and even much increased information. We term this new method optical Hall effect, because it finds simple explanation within the model described by E. H. Hall for the occurrence of the transverse and longitudinal voltages augmented by non-locality of the charge response in time. Transverse and longitudinal birefringence cause magnificent anisotropic polarization responses unraveling rich information on free charge properties of complex-structured samples due to external magnetic fields and collective movement of bound and unbound charge carriers. We demonstrate that with our technique density, type, mobility, effective mass including anisotropy can be measured without any electrical contact in buried structures, and which may have been inaccessible to any true electrical evaluation thus far. We predict a realm of applications for the optical Hall effect in future materials research and engineering.

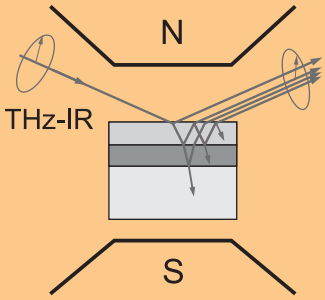

Generalized ellipsometry measures the magnetic field dependent dielectric tensor in multilayered, conductive semiconductor heterostructures and determines the free charge carrier properties of the individual sample constituents.

1 Introduction The electrical Hall effect, which has been observed by E. H. Hall in the late 70's of the 19th century, has become the standard technique for the electrical characterization of free charge carrier properties in semiconductors [1]. This technique, however, requires electrical contacts and known current paths, which excludes application to complex heterostructures and nanostructured materials. For example, the true free charge carrier properties can be obscured by space charge regions caused by the contact potentials of the electrical contacts. Furthermore, it is often difficult to determine the exact carrier path within the sample such that the free charge carrier concentrations and mobilities determined for a complex layered sample cannot be assigned separately to the individual sample constituents.

Early magnetooptic experiments in the infrared spectral range allowed access to few of the Mueller matrix informations only, and in principle permitted determination of plasma and cyclotron frequency parameters in bulk-like semiconductor samples. The early approaches are insufficient for the determination of free charge carrier properties in layered semiconductor structures [2–5]. We have shown previously that infrared magnetooptic generalized ellipsometry permits the determination of the magnetic field dependent dielectric tensor in layered semiconductor structures [6]. Here we demonstrate that generalized ellipsometry at long wavelengths when applied to conducting or semiconducting multilayer or nanoscopically in-homogeneous structures can yield equivalent and even much increased information when compared to the classical elec-

trical Hall effect [7, 8]. We term this new method optical Hall effect, because it finds simple explanation within the model described by E. H. Hall for the occurrence of static transverse and longitudinal voltages of a conducting sample placed within a magnetic field when traversed by a constant current. The principle of the optical Hall effect setup is shown in the abstract illustration. The magnetic field induced birefringence causes anisotropic polarization responses at long wavelengths which are measured using generalized ellipsometry [6, 9]. The classical model of the free charge carrier response in a magnetic field, developed by P. Drude, expands the E. H. Hall description to high-frequency optical wavelengths and holds for almost all cases relevant to semiconductor materials in complex device structures, such as laser diodes or light-emitting diodes, for example [6, 10, 11]. Here we are demonstrating the optical Hall effect on a structure of III–V semiconductor layers relevant to real device structures, such as light-emitters or transistor geometries.

2 Theory The generalized ellipsometry formalism is employed in order to determine the components of the sample constituents' dielectric tensors. The interaction between the electromagnetic plane wave and the sample is represented using the Mueller matrix calculus. In this formalism, the optical response of the birefringent sample is characterized by the 4 × 4 Mueller Matrix which relates the real valued Stokes vectors before, $\boldsymbol{S}_{\text{input}}$, and after, $\boldsymbol{S}_{\text{output}}$, the interaction with the sample: $\boldsymbol{S}_{\text{output}} = \mathbf{M}\boldsymbol{S}_{\text{input}}$ [12]. The ellipsometric data are analyzed using a stratified layer model calculation and line-shape analysis in order to determine the best-fit model parameters, for which the best match between experimental and calculated data is then achieved by varying relevant model parameters [13].

2.1 Model dielectric function At THz and far-infrared wavelength the infrared dielectric tensor $\boldsymbol{\varepsilon}(\omega)$ is composed of contributions of bound and un-bound charge oscillations. We use ensembles of Lorentz-broadened harmonic and inharmonic oscillators in order to describe the contribution of bound charge oscillations $\varepsilon^{\text{L}}(\omega)$ [14]. The contribution of the un-bound, free charge carrier excitations in an external magnetic field can be derived from Newton's equation of motion for a free charge carrier with charge q, effective mass tensor $\boldsymbol{m}^*$ and anisotropic, but energy-independent scattering rate $\boldsymbol{\gamma}$:

$$\boldsymbol{\varepsilon}^{\text{FC–MO}}(\omega) = \boldsymbol{I} + \boldsymbol{\omega}_{\text{p}}^2 \times \left[-\omega^2 \boldsymbol{I} - i\omega\boldsymbol{\gamma} + i\omega \begin{pmatrix} 0 & b_3 & -b_2 \\ -b_3 & 0 & b_1 \\ b_2 & -b_1 & 0 \end{pmatrix} \boldsymbol{\omega}_{\text{c}} \right]^{-1}, \quad (1)$$

where the external magnetic field is given by $\boldsymbol{B} = B(b_1, b_2, b_3)$ with $|\boldsymbol{B}| = B$. The the plasma frequency tensor $\boldsymbol{\omega}_{\text{p}}$ and the cyclotron frequency tensor $\boldsymbol{\omega}_{\text{c}}$ are defined as:

$$\boldsymbol{\omega}_{\text{p}}^2 = Nq^2/(\varepsilon_0 m_{\text{e}})\, \boldsymbol{m}^{*-1}, \quad (2)$$

and

$$\boldsymbol{\omega}_{\text{c}} = qB/(m_{\text{e}})\, \boldsymbol{m}^{*-1}. \quad (3)$$

Here, $\boldsymbol{m}^*$ is measured in units of the electron mass m_{e} and N is the free charge carrier density. ε_0 denotes the dielectric constant and $\boldsymbol{I}$ is the identity matrix. For the example structure described below which consists of zincblende III–V semiconductors, we assume the effective mass and the scattering tensors to be isotropic, i.e., they are described by the scalar m^* and γ, where $\boldsymbol{m}^* = m^*\boldsymbol{I}$ and $\boldsymbol{\gamma} = \gamma\boldsymbol{I}$.

2.2 p–n-structure calculation Figure 1 shows the calculated Mueller matrix difference spectra ($\Delta M_{ij} = M_{ij}(-B) - M_{ij}(+B)$) of a n-AlInP/i-GaInP/p-AlInP diode structure upon variation of the applied magnetic field B. The magnetic field is perpendicular to the sample surface and the angle of incidence is 75°. The sample structure and nominal thickness and composition values are summarized in Fig. 2. The values used for the AlInP, GaInP, and GaAs phonon frequencies and broadening parameters were determined experimentally from undoped samples with identical alloy composition. The free

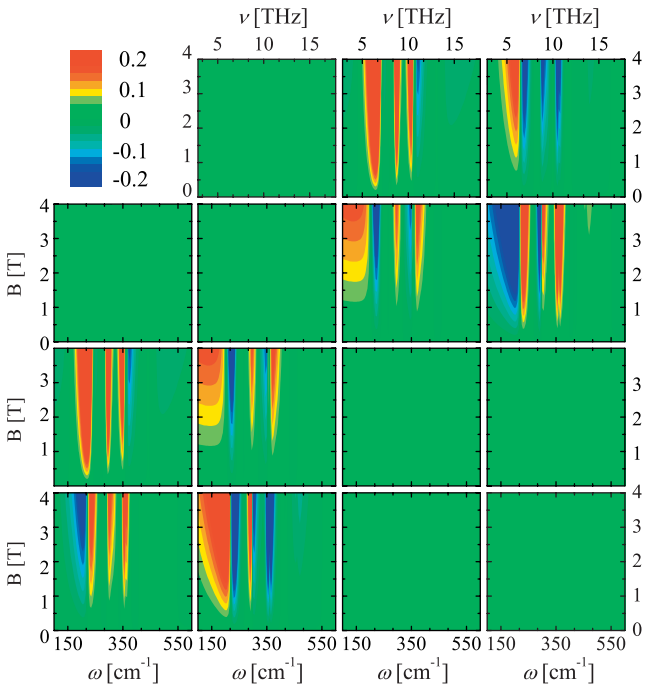

Figure 1 (online colour at: www.pss-a.com) Calculated Mueller matrix difference spectra ($\Delta M_{ij} = M_{ij}(-B) - M_{ij}(+B)$) for a p-AlInP/i-GaInP/n-AlInP diode structure as a function of the applied field B. The angle of incidence is 75°. The panels are arranged in matrix format, where each panel shows the difference spectra for the Mueller matrix element corresponding to the respective line and column index i and j.

7.	$Al_{0.49}In_{0.51}P$:Mg	264 [nm]
6.	$Al_{0.49}In_{0.51}P$	158 [nm]
5.	$Ga_{0.44}In_{0.56}P$	98 [nm]
4.	$Al_{0.49}In_{0.51}P$	27 [nm]
3.	$Al_{0.49}In_{0.51}P$:Si	395 [nm]
2.	$Al_{0.5}Ga_{0.5}As$:Si	74 [nm]
1.	GaAs:Si	207 [nm]
0.	GaAs:Si	Substrate

Figure 2 Nominal parameters of the MOVPE grown p-AlInP/i-GaInP/n-AlInP diode structure.

charge carrier parameters employed for the calculation are summarized in Table 1.

The non-zero differences in the magnetooptic Mueller matrix in the upper-right and lower-left 2×2 blocks of the Mueller matrix are directly related to the Lorenz force diverted free charge carrier movement. The elements in the 4-th row and 4-th column are antisymmetric ($M_{i4} = -M_{4i}$ for $i = (1 \ldots 3)$) whereas the remaining non-zero elements are symmetric ($M_{i3} = -M_{3i}$ for $i = (1 \ldots 3)$). The Mueller matrix difference in the upper-left and lower-right 2×2 block vanishes. This fingerprint of the optical Hall effect contains information originating from all conducting layers including the doped substrate. The anisotropic polarization response is particularly strong around 220 cm^{-1}, 300 cm^{-1}, and 350 cm^{-1}. At these frequencies interface bound waves (SGW) are excited. The SGW modes couple strongly to bulk and surface polariton modes and the spherical free charge carrier movement [15]. This results in a significantly increased sensitivity to the circularly polarized free charge carrier movement and allows the deconvolution of the contributions from the individual sample layers.

The experimental determination is often restricted to parts of the Mueller matrix, e.g., for the commonly used polarizer-sample-analyzer configuration only the upper 3×3 block of the Mueller matrix can be determined. Thus, it is desirable to distribute the optical Hall effect information over the entire Mueller matrix. This can be achieved by the introduction of a coordinate system rotation by a non-zero sample tilt along the axis defined by sample surface and plane of incidence.

Figure 3 shows the calculated Mueller matrix difference spectra obtained for identical sample parameters as in Fig. 1, but here the sample is tilted by 7° around the axis defined by sample surface and plane of incidence while the magnetic field is fixed perpendicular to the sample surface.

Table 1 Free charge carrier parameters used for the model calculations in Figs. 1 and 3.

layer	N (10^{17} cm^{-3})	m^* (m_e)	μ (cm^2/Vs)
0.	8.47	0.075	1716
1.	3.72	0.075	2500
2.	3.44	0.090	2000
3.	3.16	0.150	500
7.	3.16	0.300	300

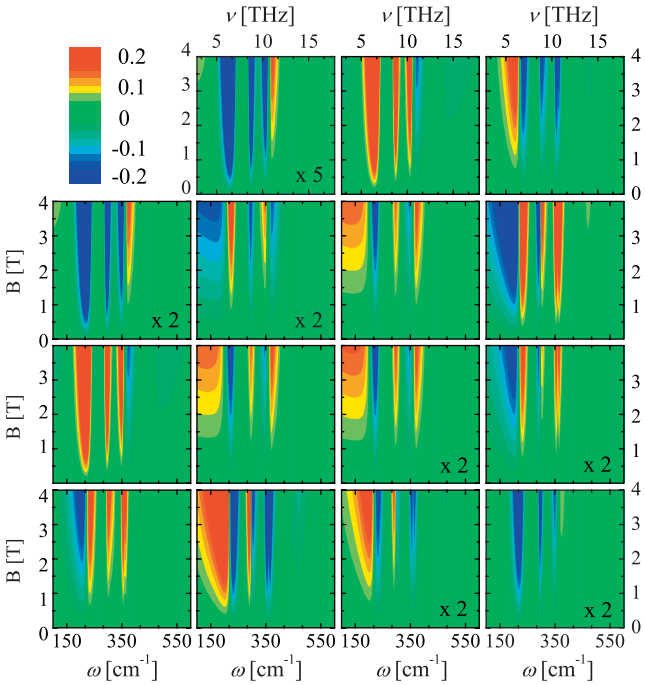

Figure 3 (online colour at: www.pss-a.com) Same as in Fig. 1 except, that the sample is tilted by 7° around the axis defined by sample surface and plane of incidence.

Experimentally the rotation can be easily achieved using the mirror configuration shown in Fig. 1 of Ref. [6]. Figure 3 shows clearly, that the optical Hall effect information is distributed over the entire Mueller matrix.

3 Experimental The experimental data have been acquired using a custom built Fourier-transform-based rotating-analyzer ellipsometer, which allows access to the upper-left 3×3 block of the samples Mueller matrix [16]. The magnetic field is normal to the sample surface. The sample is tilted by approximately 6.5° around the axis defined by sample surface and plane of incidence. For details of the experimental setup and the algorithms used for the data acquisition the interested reader is referred to Refs. [6, 16].

We investigated a multilayer p–n diode structure in order to illustrate the optical Hall effect. The structure was composed of differently doped AlInP, GaInP, and ALGaAs epi-layers which were deposited by metal organic vapor phase epitaxy (MOVPE) on top of a n-GaAs substrate. The nominal layer thicknesses and compositions are summarized in Fig. 2.

We employed a multiphase model consisting of ambient, epi-layer(s), and GaAs substrate for the model calculation. The dielectric functions of the conductive layers are composed of $\varepsilon^{FC-MO}(\omega)$ and $\varepsilon^{L}(\omega)$. All undoped layer consisted of the $\varepsilon^{L}(\omega)$ only. The parameters for the phonon frequencies were determined from un-doped layers of identical composition using far infrared spectroscopic ellipsometry and are in good agreement with literature values [17, 18].

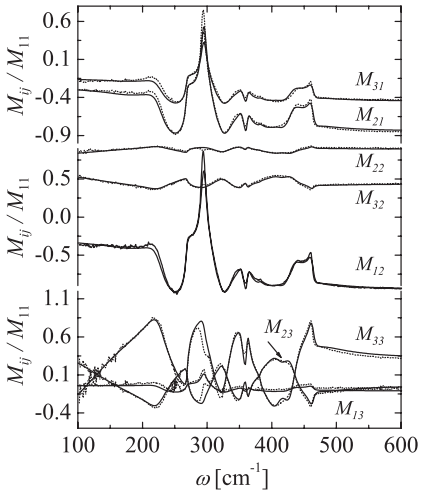

Figure 4 Zero magnetic field Mueller matrix spectra of the AlInP/GaInP/AlInP p–n-diode structure (see Fig. 2).

4 Results and discussion The magnetic field free Mueller matrix and the Mueller matrix difference spectra ($\Delta M_{ij} = M_{ij}(B = -2.10\,\mathrm{T}) - M_{ij}(B = +2.10\,\mathrm{T})$) for the diode structure are shown in Figs. 4 and 5, respectively.

The spectra in Fig. 4 are dominated by the reststrahlen bands of GaAs, AlInP, and GaInP, and allow for identification of the phonon mode frequencies of the AlP-, GaP-, and InP-like lattice vibrations, and alloy-induced modes, which are caused by residual ordering [17]. The SGW excitations can be noted most prominent at 220 cm^{-1}, 300 cm^{-1}, and 350 cm^{-1}. The spectra in Fig. 4 contain sufficient information in order to determine ω_P and γ_P of all conductive layers. ω_P and γ_P may lead to the coupled quantities N/m^* and $m^*\mu$ only [6]. This correlation can be resolved by the analysis of the optical Hall spectra in Fig. 5, which yield the different ω_c's for all conductive layers. Only the correct values for ω_c result in the precise match

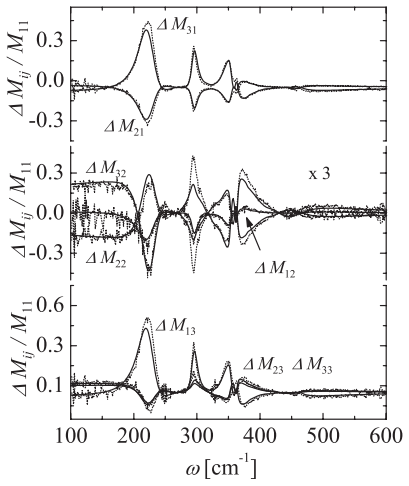

Figure 5 Mueller matrix difference spectra ($\Delta M_{ij} = M_{ij}(-B) - M_{ij}(+B)$) of the AlInP/GaInP/AlInP p–n-diode sample (see Fig. 2) for a magnetic field of $B = \pm 2.10$ T.

Table 2 Best-fit free charge carrier parameters used for the model calculations in Figs. 4 and 5. Note that the effective mass parameter in layer 2. and 7. have been fixed during the analysis.

layer	N (10^{17} cm^{-3})	m^* (m_e)	μ (cm^2/Vs)
0.	7.96	0.070	2047
1.	3.12	0.066	1896.5
2.	2.83	0.090	420
3.	2.18	0.150	340
7.	1.10	0.491	200

between the experimental and the best-model calculated data in Fig. 5 (see Eq. (1)). The combined analysis of the optical Hall effect and field free Mueller matrix data allows the unambiguous differentiation between the free charge carrier contributions summarized in Table 2. During the analysis the effective mass parameter in layer 2. and 7. have been fixed. Additional experimental data sets at variable magnetic field strengths are needed for their determination. The effective mass values for GaAs (layer 0. and 1.) and AlInP (layer 3.) are found to be in excellent agreement with literature values [19, 20].

5 Conclusion We have demonstrated the optical Hall effect as powerful tool for the determination of free charge carrier properties in layered semiconductor structures. This is exemplified using multilayered AlInP/GaInP/AlInP p–n-diode structure for which the free carrier type, density, mobility, and effective mass is determined for the individual sample constituents. We have shown that the optical Hall effect measurements contain rich information, which allow the unambiguous deconvolution of the individual free charge carrier contributions. The optical Hall effect has wide range of application in future materials research and engineering in particular were electrical determination of the free charge carrier properties is difficult because of multiple conducting layers or unresolved current paths. We envision the application of the optical Hall effect for post-growth process control of complex multilayered optoelectronic device structures.

Acknowledgements We acknowledge support from the Deutsche Forschungsgemeinschaft under grant SCHUH 1338/3-1, the National Science Foundation in MRSEC QSPIN at UNL, Startup funds from the CoE at UNL, and the J. A. Woollam Foundation.

References

[1] E. Hall, Am. J. Math. **2**, 287 (1879).
[2] M. Cardona, Phys. Rev. **121**, 752 (1961).
[3] B. Rheinländer and H. Neumann, phys. stat. sol. (b) **45**, K9 (1971).
[4] B. Rheinländer, H. Neumann, P. Fischer, and G. Kühn, phys. stat. sol. (b) **49**, K167 (1972).
[5] G. B. Wright and B. Lax, J. Appl. Phys. **32**, 2113 (1961).
[6] M. Schubert, T. Hofmann, and C. M. Herzinger, J. Opt. Soc. Am. A **20**, 347 (2003).

[7] T. Hofmann, M. Schubert, C. M. Herzinger, and I. Pietzonka, Appl. Phys. Lett. **82**, 3463 (2003).
[8] T. Hofmann, U. Schade, K. Agarwal, B. Daniel, C. Klingshirn, M. Hetterich, C. Herzinger, and M. Schubert, Appl. Phys. Lett. **88**, 42105 (2006).
[9] M. Schubert, B. Rheinländer, J. A. Woollam, B. Johs, and C. M. Herzinger, J. Opt. Soc. Am. A **13**, 875 (1996).
[10] M. Schubert, Ann. Phys. (Leipzig) **15**, 480 (2006).
[11] M. Schubert, Infrared Ellipsometry on semiconductor layer structures: Phonons, plasmons and polaritons, Springer Tracts in Modern Physics, Vol. 209 (Springer, Berlin, 2004).
[12] H. Thompkins and E. A. Irene (eds.), Handbook of Ellipsometry (William Andrew Publishing, Highland Mills, 2004).
[13] G. E. Jellison, Thin Solid Films **313/314**, 33 (1998).
[14] A. Kasic, M. Schubert, S. Einfeldt, D. Hommel, and T. E. Tiwald, Phys. Rev. B **62**, 7365 (2000).
[15] M. Schubert, T. Hofmann, and J. Šik, Phys. Rev. B **71**, 35324 (2005).
[16] T. Hofmann, U. Schade, W. Eberhardt, C. Herzinger, P. Esquinazi, and M. Schubert, Rev. Sci. Instrum. **77**, 63902 (2006).
[17] T. Hofmann, G. Leibiger, V. Gottschalch, I. Pietzonka, and M. Schubert, Phys. Rev. B **64**, 155206 (2001).
[18] T. Hofmann, V. Gottschalch, and M. Schubert, Phys. Rev. B **66**, 195204 (2002).
[19] A. Raymond, J. Robert, and C. Bernard, J. Phys. C **12**, 2289 (1979).
[20] I. Vurgaftman, J. Meyer, and L. Ram-Mohan, J. Appl. Phys. **89**, 5815 (2001).